

# Nuclear Medium Effects in the Relativistic Treatment of Quasifree Electron Scattering\*

M. Hedayati-Poor, J.I. Johansson and H.S. Sherif

Department of Physics, University of Alberta  
Edmonton, Alberta, Canada T6G 2J1

October 2, 2018

## Abstract

Non-relativistic reduction of the S-matrix for the quasifree electron scattering process  $A(e, e'p)A-1$  is studied in order to understand the source of differences between non-relativistic and relativistic models. We perform an effective Pauli reduction on the relativistic expression for the S-matrix in the one-photon exchange approximation. The reduction is applied to the nucleon current only; the electrons are treated fully relativistically. An expansion of the amplitude results in a power series in the nuclear potentials. The series is found to converge rapidly only if the nuclear potentials are included in the nuclear current operator. The results can be cast in a form which reproduces the non-relativistic amplitudes in the limit that the potentials are removed from the nuclear current operator. Large differences can be found between calculations which do and do not include the nuclear potentials in the different orders of the nuclear current operator. In the high missing momentum region we find that the non-relativistic calculations with potentials included in the nuclear current up to second order give results which are close to those of the fully relativistic

---

\*Work supported in part by the Natural Sciences and Engineering Research Council of Canada

calculation. This behavior is an indication of the importance of the medium modifications of the nuclear currents in this model, which are naturally built into the relativistic treatment of the reaction.

# 1 Introduction

Electromagnetic probes provide invaluable information about nuclear structure. The quasifree process ( $e, e'p$ ) has been used extensively to study proton hole states and to determine single particle spectroscopic factors [1]. This reaction is advantageous because the electromagnetic interaction is known; the relative weakness of the reaction permits the probe to interact almost uniformly through the entire nucleus, and the first order of perturbation theory should provide an adequate description of the process. Coincidence measurements of the ( $e, e'p$ ) reaction can provide detailed information about the single particle structure of the nucleus over a wide range of momentum transfer.

The ( $e, e'p$ ) reaction has been widely studied both non-relativistically [2, 3] and relativistically [4, 5, 6], and there are some discrepancies between the results of these investigations. Both analyses begin with a lagrangian which allows for the interaction of the photon with both electrons and protons. Non-relativistic analyses involve the reduction of the free electron-proton interaction to a form involving two-component spinors for the nucleon. This results in a hamiltonian which is expanded in powers of  $1/M$  where  $M$  is the nucleon mass [2]. The resulting interaction hamiltonian is sandwiched between Schrödinger wave functions describing the nucleons in order to form the nuclear current. Relativistic analyses are based on the Feynman diagram for one-photon exchange between the projectile electron and a proton which is imbedded in the nucleus. The electrons and nucleons are all described relativistically as spin 1/2 objects via the Dirac equation containing appropriate potentials [4, 5, 6]. A long-standing problem in quasifree electron scattering has been that the spectroscopic factors extracted from non-relativistic analyses are smaller than expected from shell model calculations. Spectroscopic factors which are found on the basis of the relativistic approach are generally larger than those found via the non-relativistic approach [4, 6].

Several groups have attempted to understand the underlying differences between these two approaches. This mainly involved looking at the sensitivity of quasifree electron scattering calculations to different optical potentials and renormalizations of the continuum wave function [7, 8, 9]. This concentration on optical potentials was largely a result of the improvement in the description of proton elastic scattering observables via Dirac phenomenology over the standard non-relativistic optical model description. Boffi et al. [7]

have multiplied the non-relativistic continuum wave function by a potential-dependent factor  $\{1 + [S(r) - V(r)] / (E + M)\}^{1/2}$ , where  $S(r)$  is the Dirac scalar potential and  $V(r)$  is the vector potential. This modification essentially changes the two-component Schrödinger wave function into the upper component of the Dirac wave function, while no other change is made in the non-relativistic calculation. They find that extracted occupation probabilities are larger than those obtained from the unmodified non-relativistic analysis. The analysis of Udias et al. [8] replaces the non-relativistic bound state wave function with the upper component of a Dirac wave function, and the non-relativistic continuum wave function is modified by factors of the same shape as the factor used by Boffi et al. The continuum wave function in this case is generated from Schrödinger-equivalent potentials [10]. The nuclear current operators are obtained in the standard way by expansion to order  $1/M^4$ . Their "non-relativistic" calculations then involve non-relativistic nuclear current operators surrounded by the upper components of Dirac wave functions. With these choices little difference is found between the relativistic and "non-relativistic" calculations. Their conclusion is that differences in observed cross sections are not due to non-relativistic reduction, but to the choice of optical potential. Jin and Onley [9] have presented a model which can take either relativistic or non-relativistic optical potentials while keeping other aspects of the calculation the same. They find that different optical potentials can change the results by as much as 14%.

These results clearly demonstrate the variability due to final state interactions, however, the issue is clouded by the occasional use of upper components of Dirac wave functions in a non-relativistic calculation. We believe that the essential difference between relativistic and non-relativistic approaches are not just in the changes in the optical potentials; these are usually phenomenological and equivalent potentials can always be found. Rather the essential difference is in the appearance of the nuclear potentials in the nuclear current operators when the relativistic amplitude is reduced to a non-relativistic form. Such medium effects on the nuclear currents are absent in the standard non-relativistic calculations.

In this paper we study the differences between the relativistic and non-relativistic approaches in calculating the amplitude for the  $(e, e'p)$  reaction. We do this through an effective Pauli reduction of the relativistic transition amplitude [11]. An expansion of the amplitude in powers of  $(E + M)^{-1}$  allows us to recover a non-relativistic limit, which matches the standard

non-relativistic calculations, with the difference that optical potentials used to generate the distorted waves are exactly equivalent to those used in the relativistic calculations. The main difference, as mentioned above is that the nuclear currents are potential dependent. We compare the two approaches and thus explain why they can still give different values for the extracted spectroscopic factors, even when equivalent optical potentials are used.

We introduce the relativistic amplitude for quasifree electron scattering in section 2. Section 3 outlines the Pauli reduction of the amplitude and some of its relevant features are discussed in section 4. The non-relativistic limit is discussed in section 5. In section 6 we compare our non-relativistic calculations with and without nuclear potentials in the nuclear current operators, to the results of the fully relativistic calculations. Our conclusions are given in section 7.

## 2 Relativistic Amplitude

We consider the one photon exchange model for the (  $e, e'p$  ) process [6], in which a photon is exchanged between the incident electron and a target proton. The struck proton is detected in coincidence with the final state electron. In this paper we are interested in the differences between the relativistic and non-relativistic treatment of the hadronic part the (  $e, e'p$  ) reaction. In the course of this discussion we do not include the Coulomb interaction in the leptonic part of the S-matrix since this will only be important for heavy nuclei [4, 12]. We will therefore not discuss any nuclei heavier than  $^{90}\text{Zr}$  in this work.

The relativistic expression for the S-matrix describing the quasifree electron scattering process (  $e, e'p$  ) in the distorted wave Born approximation (DWBA) is [6]

$$S_{fi} = \frac{-ie^2}{(2\pi)^{17/2}} \left[ \frac{M m_e^2}{E_c E_f E_i} \right]^{1/2} \sum_{J_B M_B} (J_f, J_B; M_f, M_B | J_i, M_i) \times [\mathcal{S}_{J_i J_f}(J_B)]^{1/2} \int d^4x d^4y d^4q J_{e\mu}(y) \frac{e^{-iq \cdot (x-y)}}{q^2 + i\epsilon} J_N^\mu(x), \quad (1)$$

where  $\mathcal{S}_{J_i J_f}(J_B)$  is the spectroscopic factor and  $J_e^\mu$  and  $J_N^\mu$  are electron and nuclear currents respectively.  $M$  is the nucleon mass and  $E_c$  is the energy of

the outgoing proton. The electron current is given by

$$J_e^\mu(y) = \bar{\psi}_{e_f}(y) \gamma^\mu \psi_{e_i}(y), \quad (2)$$

where  $\psi_{e_i}$  and  $\psi_{e_f}$  are the initial and final Dirac spinors for electrons. The electron wave functions are taken to be free Dirac spinors and the integration at the electron vertex can then be done analytically. This also allows the momentum integration for the photon propagator to be done, leaving one four-dimensional integration at the nucleon vertex. The nuclear current is similarly given by

$$J_N^\mu(x) = \bar{\psi}_{N_f}(x) j_N^\mu \psi_{N_b}(x), \quad (3)$$

where the nuclear current operator  $j_N^\mu$  is the choice *cc2* discussed by de Forest [13]

$$j_N^\mu = F_1(q^2) \gamma^\mu + \frac{i\kappa F_2(q^2)}{2M} \sigma^{\mu\nu} q_\nu. \quad (4)$$

$F_1(q^2)$  and  $F_2(q^2)$  are nucleon form factors and are functions of the four-momentum squared of the exchanged photon, which couples to the nucleons. We have  $q^\mu = k_i^\mu - k_f^\mu$  where  $k_i^\mu$  and  $k_f^\mu$  are the momenta of the initial and final electrons respectively. The matrix  $\sigma^{\mu\nu}$  is formed from the Dirac  $\gamma$ -matrices in the standard way as [14]

$$\sigma^{\mu\nu} = \frac{i}{2} (\gamma^\mu \gamma^\nu - \gamma^\nu \gamma^\mu). \quad (5)$$

The integration over  $d^4q$  in Eq. (1) is associated with the propagator of the exchanged photon.

The electrons are described by positive energy Dirac spinors, and the integration over coordinates at the electron vertex, in the S-matrix of equation in Eq. (1), can be done analytically to yield a Dirac  $\delta$ -function giving energy and momentum conservation at the vertex so  $q = k_i^e - k_f^e$ . The resulting  $\delta$ -function fixes the momentum of the intermediate photon so the integration over that momentum is done trivially. The integration over the time coordinate at the nucleon vertex can then be done to yield a  $\delta$ -function providing overall energy conservation. The S-matrix can then be cast in the form

$$\begin{aligned} S_{fi} = & \frac{-ie^2}{(2\pi)^{7/2}} \frac{1}{q_\gamma^2} \left[ \frac{M m_e^2}{E_c E_f E_i} \right]^{1/2} \delta(E_c + E_f - E_b - E_i) \\ & \times \sum_{J_B M_B} (J_f, J_B; M_f, M_B | J_i, M_i) \left[ \mathcal{S}_{J_i J_f}(J_B) \right]^{1/2} Z_{\nu_f \nu_i}^{\mu M_B}, \end{aligned} \quad (6)$$

where  $Z_{\nu_f\nu_i}^{\mu M_B}$  is a function of the initial and final spin projections, momenta, etc. Specifically we have at this point

$$Z_{\nu_f\nu_i}^{\mu M_B} = e_{\nu_f\nu_i}^\alpha \int d^3x \Psi_\mu^\dagger(k_p, \mathbf{x}) \Gamma_\alpha \Psi_{J_B, M_B}(\mathbf{x}) \exp(i\mathbf{q} \cdot \mathbf{x}). \quad (7)$$

where the  $4 \times 4$  matrix operating on the nucleon spinors is

$$\Gamma_\alpha = \gamma_0 \left[ F_1(q^2) \gamma_\alpha + \frac{i\kappa F_2(q^2)}{2M} \sigma_{\alpha\nu} q^\nu \right]. \quad (8)$$

The four-vector which comes from the electron vertex is

$$e_{\nu_f\nu_i}^\alpha = \left[ \frac{E_f + m_e}{2m_e} \frac{E_i + m_e}{2m_e} \right]^{1/2} \times \langle 1/2, \nu_f | \left[ 1, \frac{\boldsymbol{\sigma} \cdot \mathbf{k}_f}{E_f + m_e} \right] \gamma_0 \gamma^\alpha \left[ \frac{1}{E_i + m_e} \frac{\boldsymbol{\sigma} \cdot \mathbf{k}_i}{E_i + m_e} \right] | 1/2, \nu_i \rangle. \quad (9)$$

and this depends on the energies and momenta of the initial and final electrons as well as their spin projections. Useful details of the Fock space calculations and the expansion of the Dirac wave function in partial waves can be found in the paper by Johansson and Sherif [15]. When the appropriate factors of  $\hbar$  and  $c$  are included, the relativistic expression for the triple differential cross section is related to  $Z_{\nu_f\nu_i}^{\mu M_B}$  by

$$\begin{aligned} \frac{d^3\sigma}{d\Omega_e d\Omega_p dE_p} &= \frac{2}{(2\pi)^3} \frac{\alpha^2}{\hbar c} \left[ \frac{(m_e c^2)^2 M c^2 p_p c p_f c}{(q_\gamma c)^4 p_i c} \right] \\ &\times \sum_{J_B M_B \mu \nu_f \nu_i} \frac{\mathcal{S}_{J_i J_f}(J_B)}{2J_B + 1} |Z_{\nu_f\nu_i}^{\mu M_B}|^2, \end{aligned} \quad (10)$$

where  $\nu_i$  and  $\nu_f$  are the spin projections of the incoming and outgoing electrons respectively, while  $M_B$  and  $\mu$  are the spin projections of the bound and continuum protons.

The cross section for quasifree electron scattering in the plane wave impulse approximation can be written in a factorized form as the product of three parts [13, 2]: a kinematic factor, the cross section for the elementary process  $e + p \rightarrow e' + p'$ , which is evaluated off-shell, and finally a function of the energy and momentum of the nucleon inside the nucleus referred to as the spectral function.

In the following we will discuss results of calculations of the spectral function, proton polarization and an asymmetry parameter. The spectral function is obtained from the cross section given above by dividing by a kinematic factor and the cross section for the elementary process for  $e + p \rightarrow e + p$ . We write [13, 2]:

$$S(p_m) = \frac{\frac{d^3\sigma}{d\Omega_e d\Omega_c dE_c}}{E_c p_c \left. \frac{d\sigma}{d\Omega_e} \right|_{free}}, \quad (11)$$

where  $E_c$  and  $p_c$  are the energy and momentum of the final state proton, and  $p_m$  is the missing momentum, i.e. the momentum of the bound nucleon in the initial state. The free cross section is calculated using the nucleon current operator of Eq. (4), and is evaluated using the kinematics of the quasifree process, i.e. off-shell. Note that the experimental data are divided by the elementary cross section *cc1* of de Forest [13], while we use the nuclear current operator which leads to his cross section *cc2*, throughout this work. We are not concerned with detailed comparison with experimental data in this work, so we retain a consistent approach by using the same form for the current operator in the calculation of the quasifree S-matrix and the elementary process.

The polarization of the final state proton is given by

$$P = -2 \frac{\text{Im} \sum_{M_B \nu_f \nu_i} Z_{\nu_f \nu_i}^{1/2 M_B} \left[ Z_{\nu_f \nu_i}^{-1/2 M_B} \right]^*}{\sum_{M_B \mu \nu_f \nu_i} \left| Z_{\nu_f \nu_i}^{\mu M_B} \right|^2}. \quad (12)$$

We also define an asymmetry parameter in the missing momentum which is calculated from the differential cross sections of Eq. (10) as

$$\mathcal{A}(p_m) = \frac{d^3\sigma(p_m > 0) - d^3\sigma(p_m < 0)}{d^3\sigma(p_m > 0) + d^3\sigma(p_m < 0)}. \quad (13)$$

This asymmetry is similar to the parameter defined by Bianconi, Boffi and Kharzeev [20].

### 3 Pauli Reduction

We now perform the effective Pauli reduction [11] on the hadronic part of the amplitude only; the electrons are treated relativistically throughout. Con-



sider the nuclear current of Eq. (3) above. Using Eq. (4) one can write:

$$J^\mu(x) = \bar{\psi}_{N_f}(k_p, x) \left[ F_1(q^2) \gamma^\mu + \frac{i\kappa F_2(q^2)}{2M} \sigma^{\mu\nu} q_\nu \right] \psi_{N_b}(x). \quad (14)$$

The Dirac spinors may be written in terms of their upper components as

$$\psi_N = \left[ \frac{1}{M + E + S(r) - V(r)} \frac{\boldsymbol{\sigma} \cdot \mathbf{p}}{M + E + S(r) - V(r)} \right] u, \quad (15)$$

where  $S(r)$  and  $V(r)$  are the scalar and vector potentials, respectively, for either the bound or final state nucleons. The energy of the nucleon is  $E$ , and the associated momentum operator is  $\mathbf{p}$ . The upper component of the Dirac spinor  $u$  is related to a Schrödinger-like wave function  $\Psi_{Sch}$  by [16]

$$u = D^{\frac{1}{2}} \Psi_{Sch} \quad \text{where} \quad D(r) = \frac{E + M + S(r) - V(r)}{E + M}. \quad (16)$$

Note that the two-component wave function  $\Psi_{Sch}$  is a solution of the Schrödinger equation used in the ordinary non-relativistic calculations, i.e. containing central and spin-orbit potentials, but these potentials are "equivalent potentials" meaning that they are functions of the vector and scalar potentials of the original Dirac equation, as well as containing explicit energy dependence. For the continuum nucleon the Dirac potentials result in an improved description of nucleon-nucleus elastic scattering data [17], while for the bound state the Dirac potentials offer a slightly better description of the spin-orbit splitting than those used in earlier non-relativistic calculations [18].

The relativistic nuclear current of Eq. (14) can, with the help of Eq. (16), be written in the form

$$J^\mu = \Psi_{Sch,c}^\dagger \left\{ D_c^{1/2}(r) \left[ 1, \frac{\boldsymbol{\sigma} \cdot \mathbf{p}}{M + E_c + S_c(r) - V_c(r)} \right] \right. \\ \times \gamma^0 \left[ F_1 \gamma^\mu + F_2 \frac{i\kappa}{2M} \sigma^{\mu\nu} q_\nu \right] \\ \left. \times \left[ \frac{1}{M + E_b + S_b(r) - V_b(r)} \frac{\boldsymbol{\sigma} \cdot \mathbf{p}}{M + E_b + S_b(r) - V_b(r)} \right] D_b^{1/2}(r) \right\} \Psi_{Sch,b}. \quad (17)$$

We now perform an expansion of the object between the braces of Eq. (17). The usual representation of the Dirac  $\gamma$ -matrices is used [14] to write the  $4 \times 4$  operator in terms of  $2 \times 2$  Pauli matrices. The matrix multiplications are performed and a  $2 \times 2$  operator results. The radial function  $D^{1/2}(r)$  from Eq. (16) and the factor  $[E + M + S(r) - V(r)]^{-1}$  coming from both the bound and continuum wave functions are then expanded in powers of  $(E + M)^{-1}$ . This procedure leads to a sum of reduced nuclear current operators for each of the contributing orders:

$$J^\mu(x) = \Psi_{Sch,c}^\dagger(x) \left[ j^{\mu(0)} + j^{\mu(1)} + j^{\mu(2)} + \dots \right] \Psi_{Sch,b}(x). \quad (18)$$

The reduced current operators can be written in terms of time-like and space-like components as

$$\begin{aligned} j^{0(0)} &= eF_1, \\ j^{0(1)} &= \frac{eF_1}{2} [Q_c + Q_b], \\ j^{0(2)} &= eF_1 \left[ \frac{Q_c Q_b}{4} - \frac{Q_c^2 + Q_b^2}{8} + \frac{\boldsymbol{\sigma} \cdot \mathbf{p}}{M + E_c} \frac{\boldsymbol{\sigma} \cdot \mathbf{p}}{M + E_b} \right] \\ &\quad + \frac{\kappa F_2}{2M} \left[ \frac{\boldsymbol{\sigma} \cdot \mathbf{q}}{M + E_b} \frac{\boldsymbol{\sigma} \cdot \mathbf{p}}{M + E_c} - \frac{\boldsymbol{\sigma} \cdot \mathbf{p}}{M + E_c} \frac{\boldsymbol{\sigma} \cdot \mathbf{q}}{M + E_b} \right], \\ \mathbf{j}^{(0)} &= 0, \\ \mathbf{j}^{(1)} &= \frac{i\kappa F_2}{2M} \boldsymbol{\sigma} \times \mathbf{q} + eF_1 \left[ \frac{\boldsymbol{\sigma} \boldsymbol{\sigma} \cdot \mathbf{p}}{M + E_b} + \frac{\boldsymbol{\sigma} \cdot \mathbf{p} \boldsymbol{\sigma}}{M + E_c} \right], \\ \mathbf{j}^{(2)} &= \frac{i\kappa F_2}{4M} [Q_b + Q_c] \boldsymbol{\sigma} \times \mathbf{q} + \frac{eF_1 Q_c}{2} \left[ \frac{\boldsymbol{\sigma} \boldsymbol{\sigma} \cdot \mathbf{p}}{M + E_b} + \frac{\boldsymbol{\sigma} \cdot \mathbf{p} \boldsymbol{\sigma}}{M + E_c} \right] \\ &\quad + \frac{eF_1}{2} \left[ \frac{\boldsymbol{\sigma} \boldsymbol{\sigma} \cdot \mathbf{p}}{M + E_b} + \frac{\boldsymbol{\sigma} \cdot \mathbf{p} \boldsymbol{\sigma}}{M + E_c} \right] Q_b \\ &\quad - eF_1 \left[ Q_b \frac{\boldsymbol{\sigma} \boldsymbol{\sigma} \cdot \mathbf{p}}{M + E_b} + \frac{\boldsymbol{\sigma} \cdot \mathbf{p} \boldsymbol{\sigma}}{M + E_c} Q_c \right] \\ &\quad + \frac{\kappa F_2 q_0}{2M} \left[ \frac{\boldsymbol{\sigma} \boldsymbol{\sigma} \cdot \mathbf{p}}{M + E_b} - \frac{\boldsymbol{\sigma} \cdot \mathbf{p} \boldsymbol{\sigma}}{M + E_c} \right], \end{aligned} \quad (19)$$

where we have defined

$$Q(r) = \frac{S(r) - V(r)}{E + M}, \quad (20)$$

and the labels  $b$  and  $c$  refer to the bound and continuum states, respectively. Using the current operators from Eq. (19) up to first order in  $(E + M)^{-1}$ , in the S-matrix (1), we find that for the  $(e, e'p)$  reaction the S-matrix to first order in  $(E + M)^{-1}$  reduces to

$$\begin{aligned}
S_{fi}^{(1)} &= \frac{-ie^2}{(2\pi)^{17/2}} \left[ \frac{M m_e^2}{E_c E_f E_i} \right]^{1/2} \\
&\times \sum_{J_B M_B} (J_f, J_B; M_f, M_B | J_i, M_i) [\mathcal{S}_{J_i J_f}(J_B)]^{1/2} \\
&\times \int d^4x d^4y d^4q \frac{e^{-iq \cdot (x-y)}}{q^2 + i\epsilon} \Psi_{Sch,c}^\dagger(x) \\
&\times \left\{ J_e^0(y) F_1(q^2) \left[ 1 + \frac{1}{2}(Q_c + Q_b) \right] \right. \\
&\quad \left. - \mathbf{J}_e(y) \cdot \left[ i\kappa\mu_N F_2(q^2) \frac{\boldsymbol{\sigma} \times \mathbf{q}}{2M} \right. \right. \\
&\quad \left. \left. + F_1(q^2) \left( \frac{\boldsymbol{\sigma} \boldsymbol{\sigma} \cdot \mathbf{p}}{M + E_b} + \frac{\boldsymbol{\sigma} \cdot \mathbf{p} \boldsymbol{\sigma}}{M + E_c} \right) \right] \right\} \Psi_{Sch,b}(x). \quad (21)
\end{aligned}$$

Note that we have written this equation in a form in which the integrations over the electron coordinate and the intermediate photon momentum have not been done. The expansion method does not depend on the plane wave approximation for the electrons, and electron distortions could be included if desired. The S-matrix to second order in  $(E + M)^{-1}$  is similarly found by including the second-order nuclear current as well.

Note the dependence of the nuclear current operators on the Dirac vector and scalar potentials ( through the functions  $Q_i$  ). This dependence appears in all orders of the reduction scheme. Thus as we go to a description in terms of the Schrödinger-like wave function for the nucleon, the currents undergo a medium modification affected via the nuclear potential. This point is central to the present work. We shall discuss the traditional non-relativistic limit of the amplitude in section 5; but will concentrate in the following section on clarifying the role of the nuclear potentials in the convergence properties of the Pauli expansion of the S-matrix.

## 4 Convergence of the Expansion

In this section we discuss the convergence of the expansion obtained above to the fully relativistic calculation. In these convergence calculations, all of the factors in the expansion are the original relativistic ones. *This is not yet equivalent to a standard non-relativistic calculation!* The non-relativistic calculations are discussed below.

The calculations of the relativistic S-matrix requires knowledge of the Dirac wave functions for the bound and continuum states. For the bound state Hartree bound state wave functions are used [18]. The continuum wave functions for the knocked out proton are obtained using the energy and A dependent optical potential of Cooper *et al.* [17]. We restrict our discussion to the case of parallel kinematics [1]. In the diagrams referred to in the following discussion the curves are labelled according to their order in  $(E + M)^{-1}$  for the expansion calculations, and whether or not the Dirac potentials are included in the nuclear current operators: dotted curve – first order in  $(E + M)^{-1}$  without Dirac potentials; dashed curve – first order with potentials; dot-dashed curve – second order without potentials; dot-dot-dashed curve – second order with potentials; solid curve – fully relativistic calculation. In doing these comparisons we are attempting to clarify the convergence of the expansion and the role of the nuclear potentials ( as they appear in the nuclear currents ) in the rate of convergence of this expansion.

Figure 1 shows observables as a function of missing momentum for the reaction  $^{16}\text{O}(e, e'p)^{15}\text{N}$ , 1(a) is the spectral function while 1(b) is the proton polarization. The ground state of the residual nucleus,  $^{15}\text{N}$ , is assumed to be a  $1p_{\frac{1}{2}}$  hole. The energy of the incident electron is 456 MeV, and the kinetic energy of the detected proton is fixed at 90 MeV with parallel kinematics. The relativistic calculations of the spectral function are fitted to the peak of the data [22]; the resulting "spectroscopic factor" is then used in all the other calculations for that particular state. ( We adopt this simple fitting procedure because our main concern here is comparison between the different calculations, rather than a judicious determination of the spectroscopic factors. ) Note that the calculations with potentials included converge rapidly toward the fully relativistic results in this case, with the curve for the second order calculations being very close the relativistic results over the range of momentum transfers shown. In calculating the spectral function, the inclusion of the potential in the first order interaction terms bring the results

closer to the fully relativistic calculation than the second order without potentials. It must be stressed that the inclusion of potentials in the interaction brings the results close to the fully relativistic results, while the calculations without potentials are quite far from the relativistic results and do not show a strong indication for convergence to the relativistic result. We have also done similar calculations for the same target but leaving the residual nucleus in an excited state, as well as using different targets, namely  $^{40}\text{Ca}$  and  $^{90}\text{Zr}$ , with the residual nucleus left in both ground and excited states. These calculations show the same behavior as the calculations shown in Fig. 1. The above results are of course expected on simple mathematical grounds. The essential point however, is to shed light on the role of the appearance of the potentials in the nuclear currents. We have seen no evidence that expansions that are based on free vertices ( i.e. no nuclear potentials ), will converge to the fully relativistic results, even if calculations are done to higher order in the inverse of the nucleon mass [2]. This will have implications for the comparisons with the standard non-relativistic calculations, which we discuss next.

## 5 The Non-Relativistic Limit

The expansion of the S-matrix in powers of  $(E + M)^{-1}$  discussed above does not quite yield the amplitude used in standard non-relativistic calculations. Some care must be taken at this point in the discussion to differentiate between the correct non-relativistic limit, and the standard operator used in non-relativistic calculations. There are three things that must be done in order to obtain the proper non-relativistic limit from the relativistic amplitude:

- i) *The bound state wave function must be normalized to unity.* In the expansion obtained above, the Dirac bound state wave function is normalized to unity and the related Schrödinger-equivalent wave function is not. In the non-relativistic calculations it is the Schrödinger-equivalent wave function that must be normalized.
- ii) *The continuum wave function must be normalized correctly.* The factors arising from the Dirac field and the normalization of the Dirac wave function result in a factor of  $(E + M)/2E$  being set equal to one to obtain the non-relativistic expression for the

cross section, ( this is equivalent to multiplying the right-hand-side of Eq. (10) by the inverse of this factor ).

iii) Finally, to obtain non-relativistic expressions for the nuclear current operators from the relativistic expressions of Eq. (19), *the nucleon energies ( both continuum and bound ) are set equal to the nucleon mass, i.e.  $E \rightarrow M$ .*

It is important to note that these changes still have not yielded the standard non-relativistic amplitudes because the nuclear current operators at this stage contain the Dirac potentials explicitly. This is an essential difference between the relativistic and non-relativistic approaches, and the presence of these potentials can lead to large differences in the observables obtained via relativistic and non-relativistic approaches. In order to obtain the usual non-relativistic expression, the Dirac potentials must be removed from the nuclear current operators. When this is done, the non-relativistic equivalent of the S-matrix of Eq. (21) yields the usual first order non-relativistic transition amplitude used by many authors [2, 3]. When terms to second order are included in the non-relativistic S-matrix, and in the limit of no nuclear potentials, there are some differences between our expression and the usual non-relativistic second order S-matrix, which is obtained via a Foldy-Wouthuysen transformation of the interaction between electrons and free nucleons [2]. Fearing, Poulis and Scherer [19] have compared Foldy-Wouthuysen and Pauli reductions of a Dirac hamiltonian containing a generic potential with harmonic time dependence. They found that differences do occur beyond first order in  $1/M$ . Detailed calculations show that these differences between the Pauli and Foldy-Wouthuysen reductions are small when the nuclear potentials are ignored in the nuclear current operators. This seems the only consistent way to compare the operators since we use two different hamiltonians for the Pauli calculations.

We discuss below the effects that the presence of the potentials in the non-relativistic current operators have on calculated observables.

## 6 Results of Non-Relativistic Calculations

We now discuss results of numerical calculations using the proper non-relativistic reduction presented above. In Fig. 2. we show results for the reaction on an  $^{16}\text{O}$  target with the same kinematics as in Fig. 1. Figure 2(a) shows

the spectral function while 2(b) shows the proton polarization. The non-relativistic calculations show the same effects due to the inclusion of the nuclear potentials in the interaction operators that we saw in the corresponding convergence calculations of Fig. 1. The first and second order calculations without potentials in the nuclear currents ( dotted and dot-dashed curves respectively ) yield very similar results. This is generally true in the cases we have considered; going from first to second order in  $1/M$  does little to move the results in the direction of the relativistic calculations. When potentials are included in the nuclear currents, a large change is noticeable in going from first order to second order calculations, particularly at larger values of missing momentum. Note that the non-relativistic calculations for the spectral function converge to a lower value than the simple expansion in powers of  $(E + M)^{-1}$  ( i.e. below the relativistic calculation ). This is because the normalization of the Schrödinger-equivalent bound state wave function to unity. This results in the non-relativistic expansion converging at a point which is not the relativistic one, but a factor of the square of the inverse normalization constant lower than the fully relativistic result. This amounts to a reduction of the spectral function from the relativistic result by a factor typically in the range 1.2 to 1.4. Spin observables are not affected by changes in overall normalization, so the proton polarization calculations shown in Fig. 2(b) are very similar to those shown in Fig. 1(b), with slight differences coming from the replacement  $E \rightarrow M$  in the non-relativistic nuclear current operators.

Figure 3 emphasizes the behavior of the spectral function for the high missing momentum region of Fig. 2(a), with the missing momentum in the range 150 MeV/c to 300 MeV/c. In this region the first and second order calculations without potentials lie above the relativistic calculations, while the inclusion of potentials in first and second order moves the results to lie below the relativistic results. Note that the the relativistic calculations were fitted to the data in the low missing momentum region, but still do rather well for high missing momenta. Similar results are obtained for  $^{40}\text{Ca}$  and  $^{90}\text{Zr}$  targets, whether the residual nucleus is left in the ground or excited state. When the potentials are not included in the nuclear currents the results diverge from the relativistic calculations as the magnitude of the missing momentum is increased. On the other hand, calculations which include potentials in the nuclear current operators remain close to the relativistic results over a wide range of missing momenta. Note that we are only including terms to second order in the inverse mass.

Figure 4 shows non-relativistic calculations of the spectral function and proton polarization for the same reaction discussed in the previous figures, however in this case the energy of the incident electron is 2000 MeV, and the kinetic energy of the detected proton is fixed at 400 MeV. The larger energies allow for a much larger range of missing momenta than considered previously. It is important to note that the first and second order calculations of the spectral function, without potentials included in the nuclear current operators, differ from the relativistic calculations by up to an order of magnitude for large missing momenta, while inclusion of the nuclear potentials results in convergence to the fully relativistic results in the high missing momentum region. In addition we see that for low missing momenta the convergence point is lower than the relativistic ( see insert ). The  $(\gamma, p)$  reaction shows behavior consistent with these observations for  $(e, e'p)$  at high missing momentum [11]. The momentum transfer in the  $(\gamma, p)$  reaction is generally in the range 400 MeV/c to 600 MeV/c so these two reactions can both probe this part of the single particle bound state wave function.

Proton polarization is shown in Fig. 4(b). In the region of large missing momentum there are large differences between the polarization calculated with and without nuclear potentials in the current operator. The polarization calculated with first and second order currents containing nuclear potentials yields results close in magnitude and shape to the results of the fully relativistic calculations. Note in particular, that in the region of the minimum and maximum in the relativistic calculations close to  $p_m = -400 \text{ MeV}/c$  and  $p_m = 400 \text{ MeV}/c$  respectively, the calculations without potentials included do not reproduce the shape of the relativistic calculations at all. The potentials must be included in the nuclear current operators in order to get close to the relativistic results. In particular a measurement of the proton polarization near  $p_m = -400 \text{ MeV}/c$  provides a clear opportunity to differentiate between relativistic and non-relativistic models.

Calculation of the asymmetry parameter of Eq. (13), for small values of angular momentum  $L$  of the bound nucleon ( $L \leq 2$ ), yields similar results for all the calculations whether fully relativistic; or non-relativistic first or second order, with or without potentials in the nuclear current operator. When the angular momentum of the bound nucleon is increased, the differences between these calculations of the asymmetry become larger, as is evident in Fig. 5. The asymmetry is calculated for a  $^{90}\text{Zr}$  target, with the residual state in  $^{89}\text{Y}$



assumed to be a  $1f_{\frac{5}{2}}$  proton hole. The incident electron has an energy of 461 MeV, and the kinetic energy of the detected proton is fixed at 100 MeV. In this case the differences are particularly apparent for missing momenta in the neighborhood of 20 MeV/c.

## 7 Conclusions

In order to clarify the differences arising from relativistic and non-relativistic descriptions of quasifree electron scattering [4, 6], we have discussed an expansion of the S-matrix for the reaction  $(e, e'p)$  in powers of  $(E + M)^{-1}$  through the effective Pauli scheme. The resulting S-matrix depends on Schrödinger-like wave functions for the bound and continuum nucleons, and nuclear current operators which contain the strong Dirac potentials at the different orders. When the Dirac potentials are included in the nuclear current operators, the series essentially converges to the fully relativistic results at second order for light- to medium-mass nuclei we have considered. This indicates the importance of the role played by the nuclear potentials in the modification of the currents. When the potentials are not included in the nuclear currents, the calculations can be far from the relativistic results particularly for larger missing momenta.

These points were further studied in setting up a comparison between relativistic and non-relativistic calculations. A proper non-relativistic calculation is obtained through several steps: normalization of the bound Schrödinger-like wave function to unity, proper normalization of the continuum Schrödinger-like wave function, and in the nuclear current operators the energy of the nucleons is set equal to the nucleon mass ( i.e. take the limit  $E \rightarrow M$  ). An additional step of removing the Dirac potentials from the resulting nuclear current operators yields the standard non-relativistic amplitude. This results in a consistent and fair comparison between the relativistic and non-relativistic calculations. The potentials used for the bound and continuum protons yield both the relativistic and non-relativistic wave functions, with normalizations handled appropriately.

The non-relativistic calculations we have shown for first and second order nuclear current operators without potentials give the same results that a standard non-relativistic calculation would give if provided with the Schrödinger equivalent wave functions derived from the Dirac equation. Inclusion of the

nuclear potentials in the non-relativistic nuclear current operator results in a large change in the calculated observables. In particular, calculations of the spectral function and final proton polarization using second order nuclear current operators which include the Dirac potentials, can reproduce the magnitude and shape of the fully relativistic calculations. This is true even at large missing momenta where the non-relativistic calculations without potentials in the nuclear current operators yield very different results than the fully relativistic calculations. The polarization of the final proton is particularly sensitive to differences in the calculations, and measurements of this observable at large missing momenta could assist in the choice between the relativistic and non-relativistic approaches.

We have also calculated the asymmetry defined in the text for the different orders, with and without potentials, and found that in cases in which the angular momentum of the bound nucleon is less than 2, there are no noticeable differences between these calculations and the full relativistic. When the orbital angular momentum of the bound nucleon is greater than 2 differences between the resulting asymmetry in missing momentum of these calculations will appear. This observable thus will be useful in differentiating between relativistic and non-relativistic models only for nuclear states with large orbital angular momentum.

Other groups have examined the sensitivity of the models to changes in the optical potentials and modifications of the wave functions [7, 8, 9], and have found sensitivities at the level of 15%. However, the essential differences between the relativistic and non-relativistic approaches do not lie in modifications of the wave functions. The essential difference comes from the appearance of the nuclear potentials in the nuclear current operators; a result of the reduction of the relativistic amplitude. We emphasize that *these nuclear medium effects, characteristic of the present model, will not appear through a non-relativistic impulse description of the process.* They are, however, inherent in the relativistic description.

## Acknowledgements

We would like to thank J.M. Udias and L. Lapikás for useful correspondence regarding quasifree electron scattering.

## References

- [1] S. Frullani and J. Mougey, *Advances in Nuclear Physics*, edited by J.W. Negele and E. Vogt, **14** (1984) 1.
- [2] S. Boffi, C. Giusti and F.D. Pacati, Nucl. Phys. **A336** (1980) 416; Nucl. Phys. **A336** (1980) 427.
- [3] K.W. McVoy and L. Van Hove, Phys. Rev. **125** (1962) 1034.
- [4] J.P. McDermott, Phys. Rev. Lett. **65** (1990) 1991.
- [5] Y. Jin, D.S. Onley and L.E. Wright, Phys. Rev. C **45** (1992) 1311.
- [6] J.M. Udias, P. Sarriguren, E. Moya de Guerra, E. Garrido and J.A. Caballero, Phys. Rev. C **48** (1993) 2731.
- [7] S. Boffi, C. Giusti, F.D. Pacati and F. Cannata, Il Nuovo Cimento **98A** (1987) 291.
- [8] J.M. Udias, P. Sarriguren, E. Moya de Guerra, E. Garrido and J.A. Caballero, NIKHEF-K preprint numbers NIKHEF-93-P12 and FNIEM-13.
- [9] Yanhe Jin and D.S. Onley, Phys. Rev. C **50** (1994) 377.
- [10] H.S. Sherif, R.I. Sawafta and E.D. Cooper, Nucl. Phys. **A449** (1986) 709.
- [11] M. Hedayati-Poor and H.S. Sherif, Phys. Lett. **B326** (1994) 9.
- [12] C. Giusti and F.D. Pacati, Nucl. Phys. **A473** (1987) 717.
- [13] T. de Forest Jr., Nucl. Phys. **A392** (1983) 232.
- [14] J.D. Bjorken and S.D. Drell, *Relativistic Quantum Mechanics*, McGraw-Hill Book Company (1964).
- [15] J.I. Johansson and H.S. Sherif, Nucl. Phys. **A575** (1994) 477.
- [16] B.C. Clark, S. Hama, R.L. Mercer, AIP conf. proc. No. **97**, ed: H.O. Mayer (1982) 260; J. Raynal, Aust. J. Phys. **43** (1990) 9; G.Q. Li, J. Phys. **G19** (1993) 1841.

- [17] E.D. Cooper, S. Hama, B.C. Clark and R.L. Mercer, Phys. Rev. C **47** (1993) 297.
- [18] C.G. Horowitz and B.D. Serot, Nucl. Phys. **A368** (1986) 503.
- [19] H.W. Fearing, G.I. Poulis and S. Scherer, Nucl. Phys. **A570**, (1994) 657.
- [20] A. Bianconi, S. Boffi and D.E. Kharzeev, Phys. Rev. C **49** (1994) 1243.
- [21] H.S. Sherif, R.I. Sawafta and E.D. Cooper, Nucl. Phys. **A449** (1986) 709.
- [22] L. Lapikás, Nucl. Phys. **A553** (1993) 297.

## Figure Captions

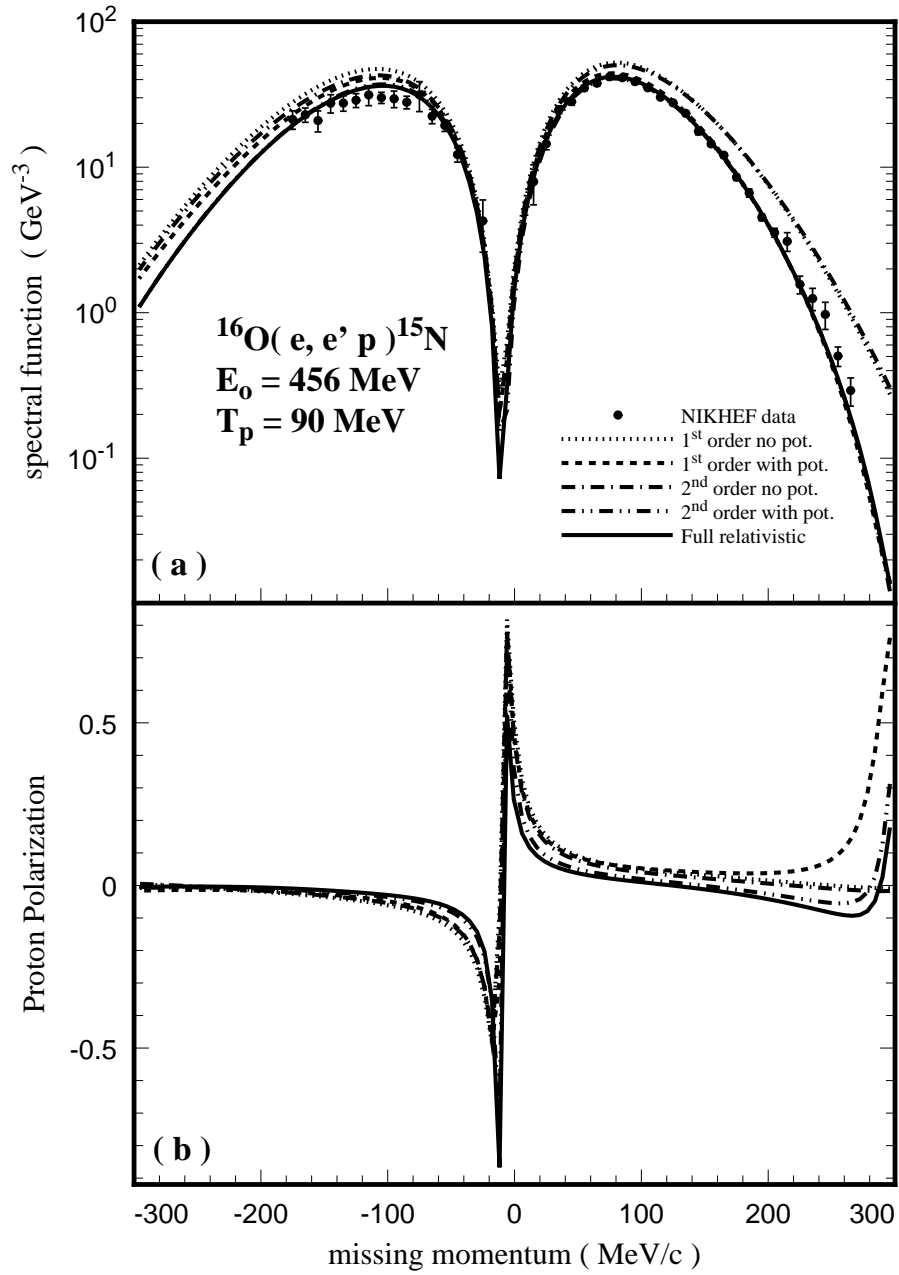
FIG. 1. Observables for the reaction  $^{16}\text{O}(e, e'p)^{15}\text{N}$  where  $^{15}\text{N}$  is in the  $1p_{\frac{1}{2}}$  state. The energy of the incident electron is 456 MeV, and the kinetic energy of the detected proton is fixed at 90 MeV with parallel kinematics. Hartree bound state wave functions are used [18] and the proton optical potentials are from [17]. The data are from reference [22]. (a) spectral function and (b) proton polarization. Curves labelled according to their order in  $(E + M)^{-1}$  and whether or not the Dirac potentials are included in the nuclear current operators: dotted curve – first order in  $(E + M)^{-1}$  without Dirac potentials; dashed curve – first order with potentials; dot-dashed curve – second order without potentials; dot-dot-dashed curve – second order with potentials; solid curve – fully relativistic calculation.

FIG. 2. Observables for the reaction  $^{16}\text{O}(e, e'p)^{15}\text{N}$  where  $^{15}\text{N}$  is in a  $1p_{\frac{1}{2}}$  proton hole state. The kinematics are those of Fig. 1. Curves labelled according to their order in  $1/M$  and whether or not the Dirac potentials are included in the nuclear current operators: dotted curve – non-relativistic calculations, first order in  $(E + M)^{-1}$  without Dirac potentials; dashed curve – first order with potentials; dot-dashed curve – second order without potentials; dot-dot-dashed curve – second order with potentials; solid curve – fully relativistic calculation. Potentials and data from the sources of Fig. 1.

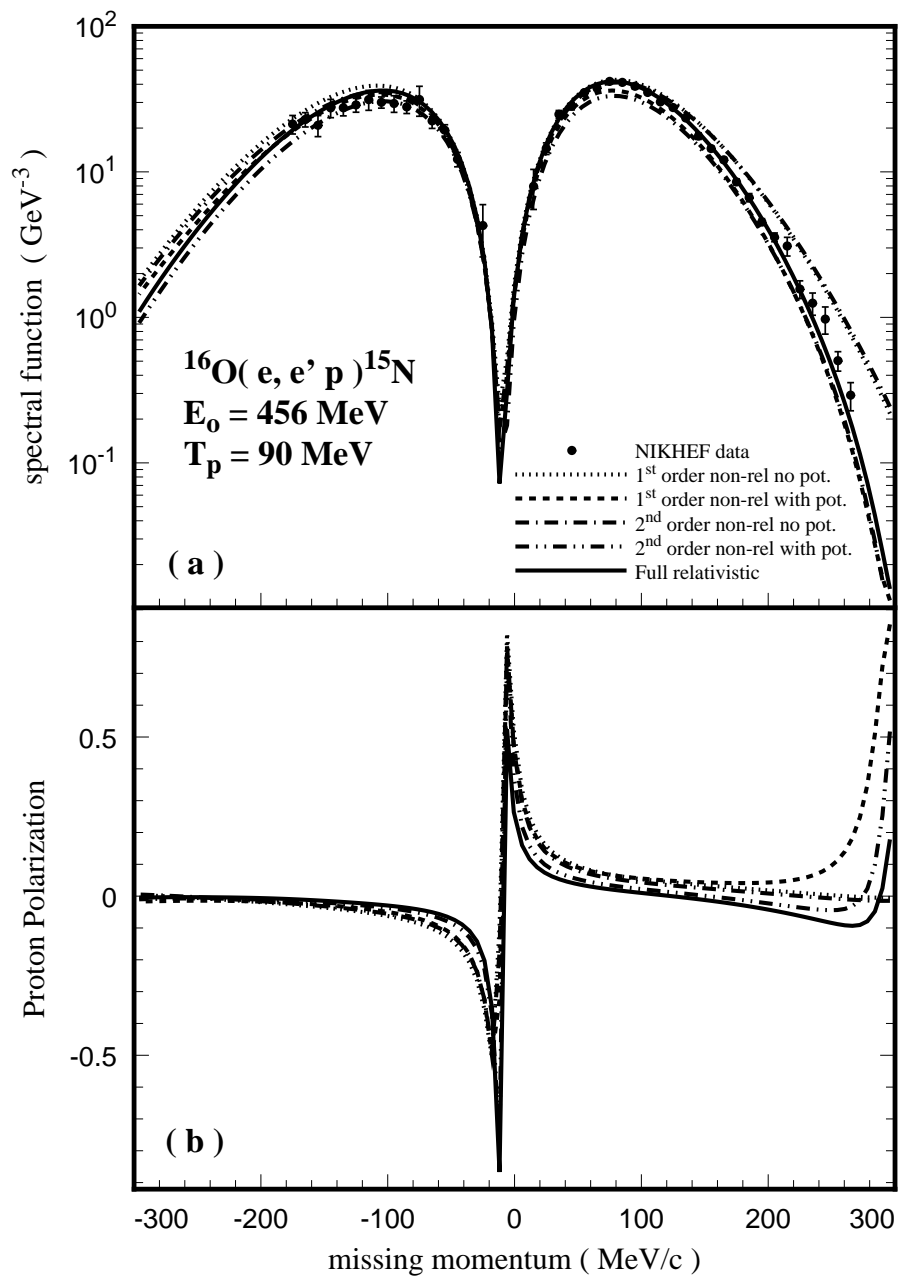
FIG. 3. Spectral function for  $^{16}\text{O}(e, e'p)^{15}\text{N}$  where  $^{15}\text{N}$  is in the  $1p_{\frac{1}{2}}$  state. The kinematics are those of Fig. 1. Curves labelled as in Fig. 2. Potentials and data from the sources of Fig. 1.

FIG. 4. Observables for  $^{16}\text{O}(e, e'p)^{15}\text{N}$  where  $^{15}\text{N}$  is in the  $1p_{\frac{1}{2}}$  state. The energy of the incident electron is 2000 MeV, and the kinetic energy of the detected proton is fixed at 400 MeV with parallel kinematics. Curves labelled as in Fig. 2. Potentials from the source of Fig. 1.

FIG. 5. Asymmetry in missing momentum for  $^{90}\text{Zr}(e, e'p)^{89}\text{Y}$  where  $^{89}\text{Y}$  is in the  $1f_{\frac{7}{2}}$  state. The energy of the incident electron is 461 MeV, and the kinetic energy of the detected proton is fixed at 100 MeV with parallel kinematics. Curves labelled as in Fig. 2. Potentials from the source of Fig. 1.



**Figure 1**  
**M. Hedayati-Poor**



**Figure 2**  
**M. Hedayati-Poor**

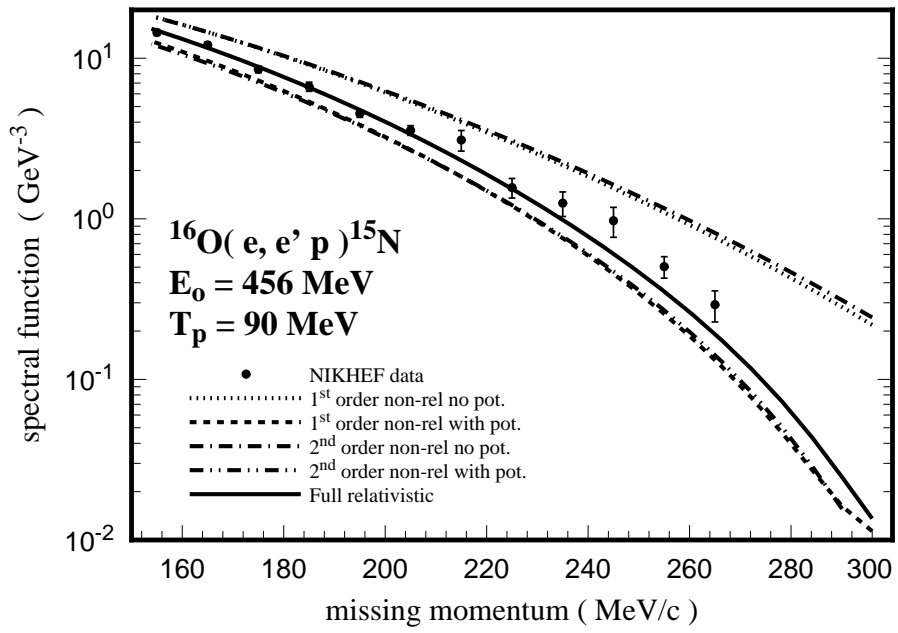


**Figure 3**  
**M. Hedayati-Poor**



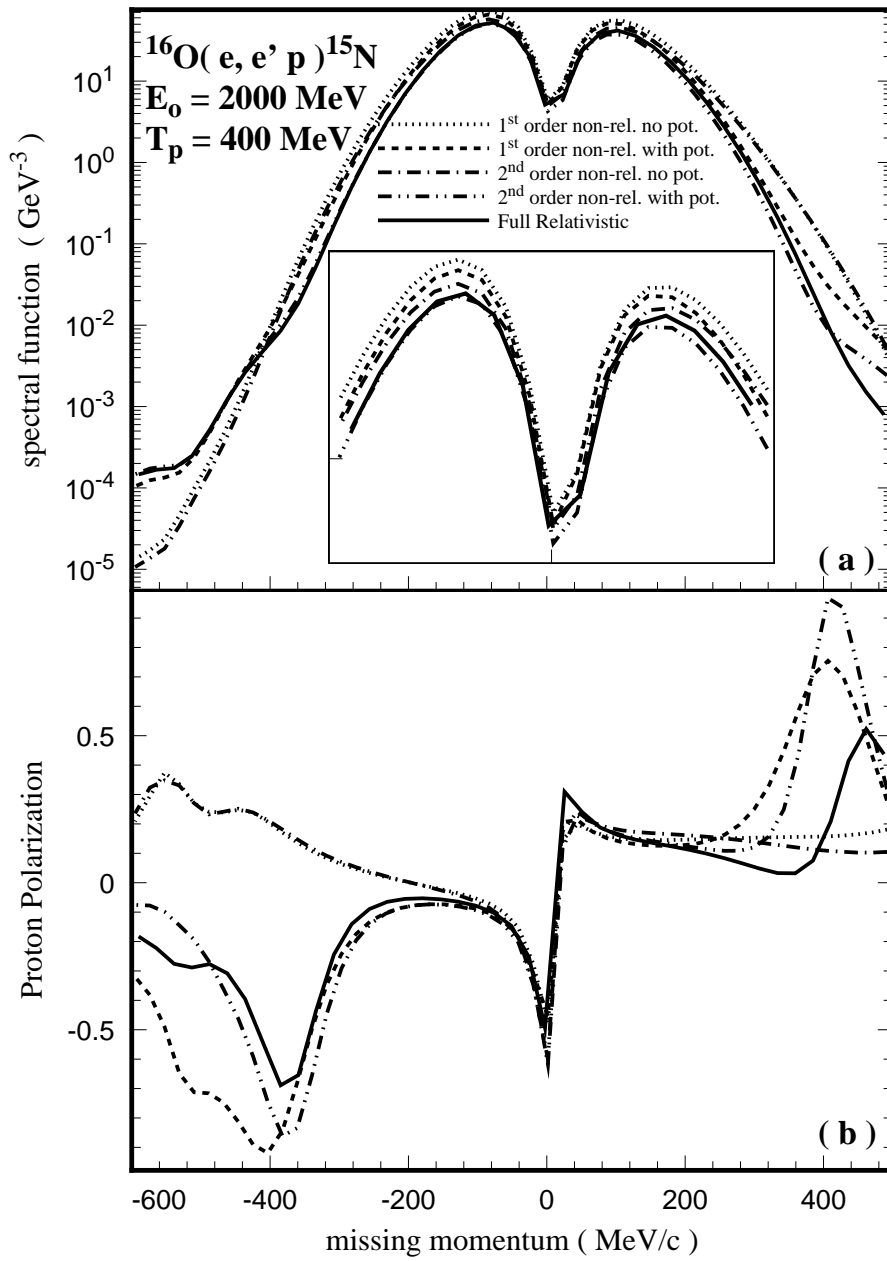


**Figure 4**  
**M. Hedayati-Poor**

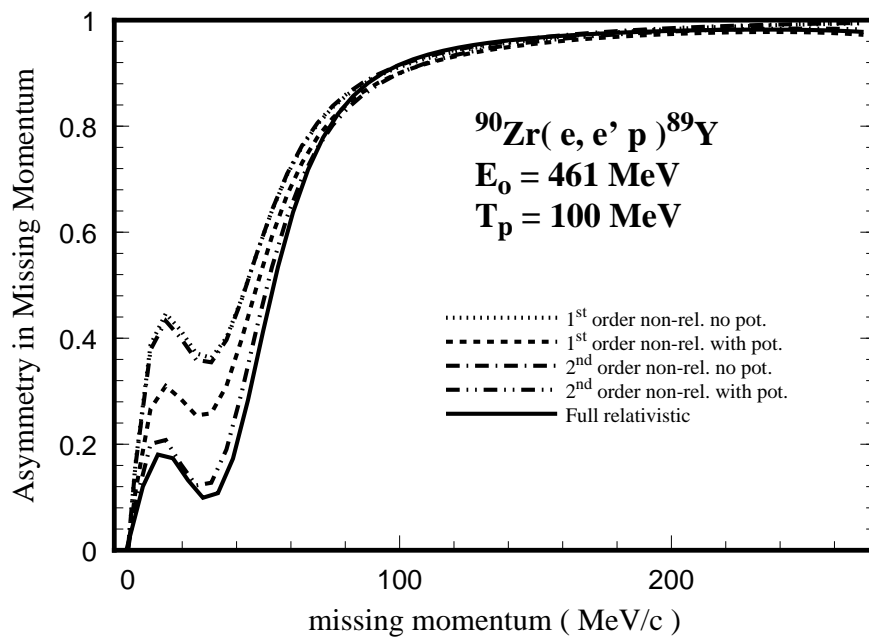


**Figure 5**  
**M. Hedayati-Poor**